Fabrication and Replication of Arrays of Single- or Multicomponent Nanostructures by Replica Molding and Mechanical Sectioning

Darren J. Lipomi,[†] Mikhail A. Kats,[‡,§] Philseok Kim,[†,‡,§] Sung H. Kang,[‡] Joanna Aizenberg,[†,‡] Federico Capasso,[‡] and George M. Whitesides[†,*]

[†]Department of Chemistry and Chemical Biology and [‡]School of Engineering and Applied Sciences, Harvard University, 29 Oxford Street, Cambridge, Massachusetts 02138. [§]These authors contributed equally to this work.

ABSTRACT This paper describes the fabrication of arrays of nanostructures (rings, crescents, counterfacing split rings, cylinders, coaxial cylinders, and other structures) by a four-step process: (i) molding an array of epoxy posts by soft lithography, (ii) depositing thin films on the posts, (iii) embedding the posts in epoxy, and (iv) sectioning in a plane parallel to the plane defined by the array of posts, into slabs, with an ultramicrotome ("nanoskiving"). This work demonstrates the combination of four capabilities: (i) formation of structures that are submicrometer in all dimensions; (ii) fabrication of 3D structures, and arrays of structures, with gradients of height; (iii) patterning of arrays containing two or more materials, including metals, semiconductors, oxides, and polymers; and (iv) generation of as many as 60 consecutive slabs bearing contiguous arrays of nanostructures. These arrays can be transferred to different substrates, and arrays of gold rings exhibit plasmonic resonances in the range of wavelengths spanning 2—5 μm.

KEYWORDS: nanoskiving · nanofabrication · plasmonics · metamaterials · soft lithography · ultramicrotomy

The interaction of electromagnetic fields with metallic nanostructures can produce collective oscillations of the conduction electrons at metal—dielectric interfaces. These oscillations are known as localized surface plasmon resonances (LSPRs) and propagating surface plasmon polaritons (SPPs) and are responsible for most of the phenomena in the field of plasmonics.[1] Two- and three-dimensional arrays of metallic nanostructures could play key roles in functional materials. Optical filters,[2,3] substrates for optical detection of chemical and biological analytes using LSPRs[4] or surface-enhanced Raman scattering (SERS),[5−7] substrates for enhanced luminosity,[8] materials to augment absorption in thin-film photovoltaic devices,[9,10] metamaterials[11,12] with negative magnetic permeabilities[13] and negative refractive indices,[14] and surfaces for perfect lenses[15] and invisibility cloaking[16] are examples of possible and realized applications. There are, however, significant technical challenges in generating arbitrary patterns of metallic, dielectric, and semiconducting nanostructures for research and for potential commercial devices. The most sophisticated patterns are fabricated using electron-beam lithography (EBL),[17] focused-ion beam (FIB) milling and lithography,[14] or direct laser writing.[18] These techniques can generate nearly arbitrary patterns in resists (*e.g.*, EBL) or hard materials (*e.g.*, FIB milling), but they are serial, expensive, and require access to a cleanroom.

A number of techniques have emerged that have begun to address the challenges associated with conventional scanning-beam lithographic tools.[19] Xia and co-workers recently reviewed synthetic methods that can produce large quantities of high-quality metallic structures for plasmonic applications.[20] These materials, however, are difficult to arrange in the ordered arrays that are required for many applications in optics.[21] Van Duyne and co-workers have developed an approach to generate ordered arrays of metallic particles called "nanosphere lithography", which uses a monolayer of colloidal crystals as a stencil mask; the triangular voids direct the deposition of metal on the substrate by evaporation.[22] Giessen and co-workers used the same voids as apertures through which to produce split-ring resonators by rotating the substrate at an angle during evaporation.[23] The laboratories of Rogers, Odom, Nuzzo, and others have used soft lithographic processes to fabricate large-area patterns of metallic nanostructures.

See the accompanying Perspective by Wiley *et al.* on p 3554.

*Address correspondence to gwhitesides@gmwgroup.harvard.edu.

Received for review May 6, 2010 and accepted May 26, 2010.

Published online June 8, 2010.
10.1021/nn100993t

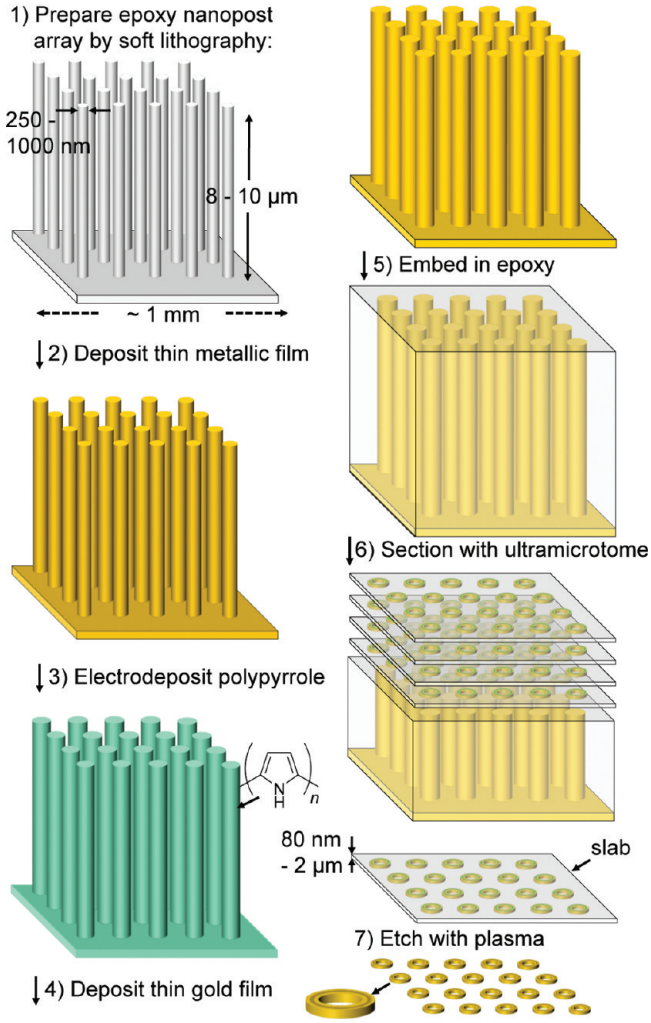

Figure 1. Summary of the procedure used to fabricate concentric rings by thin-film deposition and thin sectioning of high-aspect-ratio nanoposts.

These processes include phase-shifting edge lithography[24] and molding UV-curable imprint resists with transparent poly(dimethylsiloxane) (PDMS) stamps[25] to form arrays of plasmonic nanostructures, such as arrays of apertures in metallic films[26] or pyramidal shells.[27]

One particular challenge among methods of fabrication is the ability to generate patterns comprising two or more materials (such as metals, semiconductors, and dielectrics) in the same plane. Multicomponent patterns would be useful for building metamaterials and other optical devices. Tserkezis *et al.* produced arrays of sandwich-like, metal−dielectric−metal nanostructures, which exhibited negative magnetic permeabilities when exposed to visible and near-IR radiation,[28] while Su *et al.* used the same type of structures as substrates for efficient SERS.[29] Engheta has recently described optical nanocircuits inspired by metamaterials, in which patterns of mixed metallic and dielectric structures behave as nanoinductors and nanocapacitors, in close analogy to microelectronic systems.[30] Top-down patterning of vertical stacks of alternating layers of materials has been the principal method used to fabricate multimaterial optical nanostructures. The use of focused-electron-beam (FEB) deposition, or FIB milling, to produce patterns comprising two or more materials in the same plane is possible, in principle,[31] but it has not been developed.

Nanoskiving is a process whose key step is thin sectioning with an ultramicrotome.[32] When combined with soft lithography and thin-film deposition, it introduces "cutting" as a method of replicating patterns that is complementary to the established techniques of printing and molding.[33] It converts the perimeters of molded relief features into the geometries of the nanostructures (see Figure 1). The procedure used for the two-dimensional patterning required to create the three-dimensional master determines the geometry of the features; the thicknesses of the thin films determine the line widths of the features; and the ultramicrotome determines the height of the features (30−2000 nm). In previous work, Xu *et al.* fabricated arrays of open and closed-loop structures of gold using a process that combined photolithography, replica molding, and nanoskiving.[34] These arrays served as mid-IR, frequency-selective surfaces. The structures had relatively large outer diameters (2 μm) and were sectioned from an embedded structure with relatively shallow relief (~2 μm); this topography did not allow a large number of cross sections to be made. The ability to generate a large number of copies (>20) of structures that are submicrometer in all dimensions requires reusable, high-aspect-ratio masters of the type that can be made by EBL followed by deep reactive-ion etching (DRIE).[35]

Soft lithographic molding has improved dramatically in the past few years, in terms of both the absolute sizes and aspect ratios of molded features that it can generate. For example, (PDMS), molded over a crack in a silicon wafer, replicated a step height of 0.4 nm.[36] We have shown earlier that replica molding can be used to transfer an array of high-aspect-ratio nanoposts from silicon to epoxy, through a PDMS intermediate.[35] Here we show that, in combination with nanoskiving, these high-aspect-ratio structures provide a basis for the fabrication of arrays of significantly smaller and more complex structures, and in greater numbers of replicas, than has been possible previously.

Mastering and Molding. We obtained a silicon master bearing an array of cylindrical posts by EBL followed by Bosch DRIE.[37] The total area of the array was ≥1 cm^2. We replicated these arrays of cylindrical posts in a UV-curable epoxy using a PDMS mold as an intermediate.[35]

Materials. Many methods of fabrication focus on structures of gold because it has useful plasmonic and electronic properties, it does not oxidize under ambient conditions, and it is easily deposited by evaporation.[19] To demonstrate that our process could be used with materials in addition to gold, we formed nanostructures of silver, silicon, palladium, platinum, silicon dioxide,

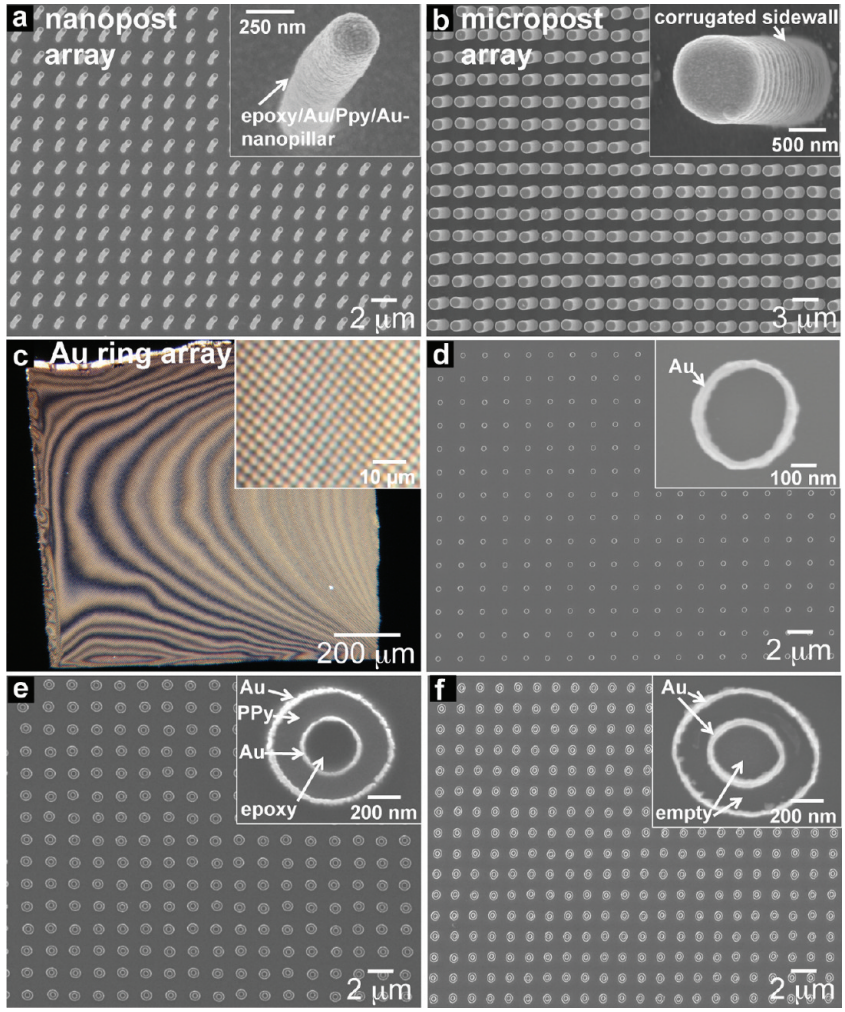

Figure 2. Scanning electron microscope (SEM) images (a,b,d−f) and optical images (c) of arrays of structures, before and after nanoskiving. (a) Array of nanoposts after conformal coating with gold (Au), polypyrrole (PPy), and gold. (b) Array of microposts bearing corrugated side walls. (c) A ~1 mm^2 array of Au microrings. The interference-like pattern across the array is due to the corrugated side walls of the master used. The diameters of the rings are ~10% larger in the bright regions than they are in the dark regions, as determined by SEM. The inset is a high-magnification image of the features. (d) Two-dimensional array of single Au rings. (e) Array of concentric Au rings separated by a layer of electrochemically grown PPy. (f) Array of concentric Au rings after etching the organic components.

the conducting organic polymer poly(pyrrole) (PPy), and films of lead sulfide (PbS) nanocrystals. We also demonstrated the ability to fabricate structures of two or more materials in the same array.

Deposition of Thin Films. We deposited conformal films of metal on the nanoposts using a benchtop sputter-coater. In many cases, it was desirable to leave regions of the nanoposts unmetalized, for example, when making split rings. In these situations, we used electron-beam evaporation. Evaporation produces a collimated beam of metal atoms, which metalizes only the side walls of topographic features in its path. We deposited PPy films by electrodeposition and films of PbS nanocrystals by drop-casting.

Nanoskiving. To produce two-dimensional arrays, we sectioned most blocks into slabs ~1 mm^2 in area and 80−150 nm thick, under ambient conditions. To produce quasi-three-dimensional arrays, very high-aspect-ratio structures, and wedge-shaped slabs, we cut slabs up to 2 μm thick. We used a 35° diamond knife, which sections materials with less compression than does a (more common) 45° knife.[38,39] We used a UV-curable epoxy (UVO-114, obtained from Epoxy Technology Inc.) because of its strong adhesion to metals, and resistance to compression during sectioning.

Measurement and Simulation. We transferred our nanostructures onto chemically vapor-deposited ZnSe, which is a common substrate for infrared applications. It has a wide band of transmission spanning wavelengths from 500 nm to 20 μm (which includes the region in which we expected the nanostructures to resonate) and a refractive index around 2.4 at near- to mid-IR frequencies. We characterized some of the structures produced by this method using Fourier transform infrared (FTIR) spectroscopy in transmission mode. We compared the experimental spectra to those calculated by the finite-difference time-domain (FDTD) method, a standard technique

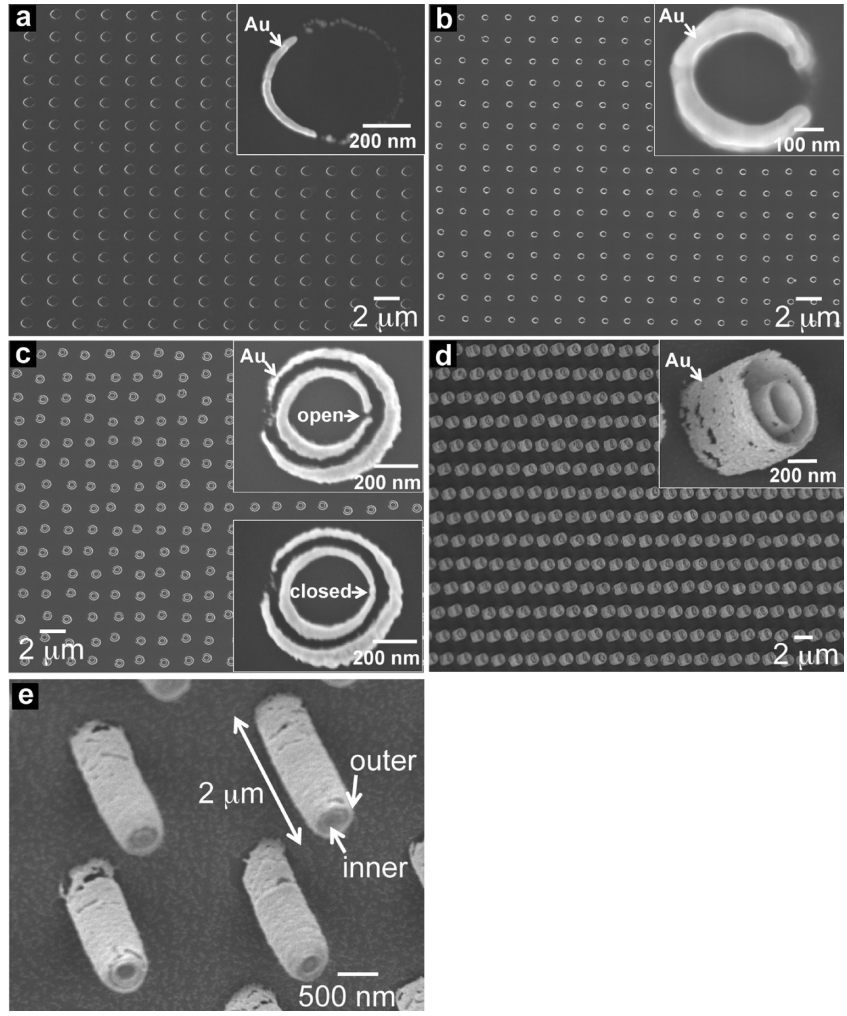

Figure 3. SEM images of two-dimensional (2D) arrays of gold nanostructures. (a) Gold crescents. (b) Gold split rings. (c) Concentric split rings. The array contains a mixture of the two structures shown in the insets. (d) High-aspect-ratio concentric rings (image obtained at 45°). (e) Very high-aspect-ratio coaxial cylinders of gold.

for solving Maxwell's equations in the time domain.[40,41]

RESULTS AND DISCUSSION

Fabrication of Nanopost Arrays. We created two types of arrays of epoxy posts. The first ("nanoposts") was a square array with $d \sim 250$ nm, $h = 8$ μm, and pitch $= 2$ μm. The array covered 1 cm^2 (though we would only be able to cut slabs with sides ≤2.4 mm because that was the length of our diamond knife). The second master ("microposts") had features with $d \sim 1$ μm, $h = 9$ μm, and pitch $= 3$ μm. The array covered 8 cm^2. We found that the silicon masters could be used indefinitely to prepare PDMS molds, which, in turn, could produce multiple epoxy replicas.

Fabrication of Arrays of Metallic Nanostructures by Sectioning Nanoposts Bearing Metallic Films. Figure 1 summarizes the procedure used to generate arrays of nanoposts coated with two gold films, separated by a film of conducting polymer. We began by sputter-coating an array of nanoposts with gold (step 1). This film served as the working electrode for the conformal electrodeposition of PPy (step 2). A second deposition of gold provided an array of four-component, coaxial nanoposts (step 3). We embedded this structure in additional epoxy to form a block (step 4). Sectioning this block yielded epoxy slabs containing the nanostructures (step 5). The slabs could be transferred from the water bath on which they floated to a wide variety of substrates (not shown).[42] Treatment with an air plasma removed both the epoxy matrix and the PPy between the gold rings (step 6). Figure 2a,b shows arrays of nanoposts and microposts before sectioning. The microposts had scalloped side walls; this topography is a trait of the Bosch DRIE process used to produce the silicon master. The corrugated side walls (scalloping) had a period of ~400 nm and an amplitude of ~100 nm. We were able to smooth the side walls of the posts and to create posts with thinned or thickened diameters, without fabricating a new silicon master, by etching or coating an epoxy replica and reusing it as a master (see Supporting Information). Figure 2c shows a dark-field optical image of an array of

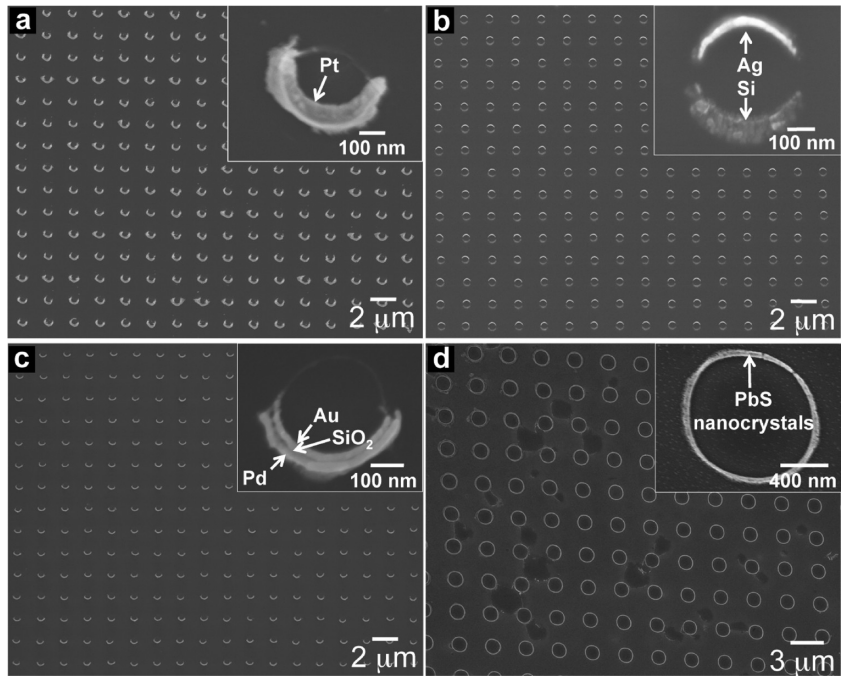

Figure 4. SEM images of 2D arrays of multicomponent nanostructures. All structures are 80−100 nm in height. (a) Crescents of platinum. (b) Counterfacing crescents of silver and silicon. (c) Crescents of gold and palladium separated by a layer of silicon dioxide. (d) Microrings composed of PbS nanocrystals, which are continuous around the circumference of the rings.

gold rings covering an area of ~1 mm^2. Figure 2d shows a scanning electron microscope (SEM) image of an array of gold rings.

Fabrication of Concentric Rings of Gold. We obtained concentric rings of gold separated by PPy by following the procedure summarized in Figure 1. Figure 2e is an image of the array of these discs, which are embedded in an epoxy matrix. Figure 2f is an image of concentric rings separated by empty space, created by etching the organic components of the structures shown in Figure 2e. To determine the yield of the process, we obtained an array by sectioning a 140 nm thick slab of these structures over an area of 1 mm^2. We chose a random region 2000 μm^2 in area (which contained 486 concentric rings) and counted the defective structures by SEM. The yield of unbroken structures was 485 (99.8%). Broken structures had gaps in the rings. Ten structures (2%) appeared to have a metal fragment bridging the two gold rings (see Supporting Information, and Figure S6, for details).

Number of Sections. To determine the number of sections we could obtain from a single block of nanoposts, we cut through an 8 μm tall, 1 mm^2 in area, array of nanoposts in 100 nm increments (the maximum number of perfect slabs would be 80). We counted 27 consecutive slabs in which at least 90% of the area defined by the slab was covered by a contiguous array of nanostructures, and 60 slabs (including the first 27) in which at least 50% of the area was covered, as estimated by optical microscopy. We attribute the loss in yield to the imperfect, manual alignment of the embedded nanoposts with the diamond knife. Fiduciary markers within the epoxy block or an automated alignment system would increase the yield of replications.

Fabrication of Crescents and Split Rings. Using a modification of the procedure shown in Figure 1, it was possible to obtain arrays of gold crescents and split rings. We began with an array of epoxy nanoposts, but instead of coating the nanoposts conformally, we deposited only partially around the circumferences of the nanoposts by shadow evaporation. Placement of the substrate at a 45° angle from the source of evaporation afforded the array of crescents shown in Figure 3a. Iterative evaporation and rotation of the substrate in the evaporator produced the array of split rings shown in Figure 3b.

Fabrication of Counterfacing Concentric Split Rings. Counterfacing, concentric split-ring resonators have been predicted to have negative effective magnetic permeabilities and are thus a possible component of negative-index metamaterials.[13] Shadow evaporation and rotation of the nanopost array within the evaporator produced a gold film around the nanoposts in the form of split cylinders. Electrodeposition of PPy, which bridged the opening and controlled the spacing between the two counterfacing split rings, followed by another metallization oriented 180° to the first, formed a second split cylinder enclosing the first. Nanoskiving this array produced counterfacing split rings (Figure 3c). The array shown is a mixture of the two types of structures shown in the insets: counterfacing split rings and structures in which the inner ring is closed.

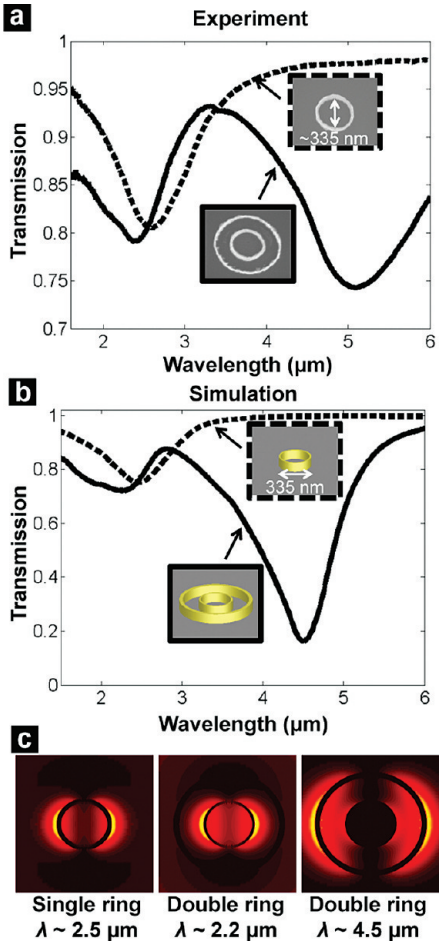

Figure 5. Comparison of transmission spectra of arrays of gold nanostructures produced by nanoskiving, and FDTD simulations of the nanostructures with idealized geometries. (a) Transmission spectra as a function of free-space wavelengths for two types of arrays of gold nanostructures (area ~ 0.5 mm^2) mounted on a ZnSe substrate. (b) Corresponding simulated spectra (FDTD) of 5 × 5 arrays, for which we assumed the rings were identical and exactly circular. (c) Simulated near-field profiles of intensity of the electric field, viewed as a cross section through the center of the rings. The wavelengths of incident light that excite these modes correspond to the dips in transmission in (b).

Fabrication of High-Aspect-Ratio Structures. One of the advantages of nanoskiving is that it can produce high-aspect-ratio structures, by cutting micrometer-thick slabs (up to 10 μm thick is possible with an ultramicrotome). Figure 3d shows an array of high-aspect-ratio concentric cylinders obtained by cutting a 600 nm thick slab from an array of posts, such as those shown in Figure 2a. A 20 min exposure to an air plasma (100 W, 1 torr) etched the epoxy matrix and the PPy between the two gold shells. Figure 3e is an array of coaxial cylinders with very high aspect ratios. Even the tallest structures in the array (~2 μm, as shown in Figure 3e) did not fall over.

Fabrication of Nanostructures of Other Materials. In order to show that it was possible to produce structures of materials other than gold, we formed crescents of platinum (Figure 4a). We also formed opposing crescents of silver and silicon (Figure 4b) and an array of crescents composed of gold, silicon dioxide, and palladium (Figure 4c) to demonstrate the formation of patterns comprising precisely registered (or touching) nanostructures of two or more materials. Nanoskiving is not limited to structures deposited by physical vapor deposition. Semiconductor nanocrystals can be coated on the side walls of epoxy posts and sectioned into arrays of rings. Drop-casting a solution of oleylamine-capped PbS nanocrystals in hexanes on an array of epoxy microposts, followed by plasma oxidation of the ligands (which rendered the film insoluble),[43] embedding the array in epoxy, and sectioning, produced the array of rings shown in Figure 4d.

Transmission Spectra of Arrays of Single and Double Rings. In order to demonstrate that the arrays of nanostructures produced by nanoskiving are of sufficient quality for optical applications, we obtained transmission spectra of an array of single rings and double, concentric rings (Figure 5) on a ZnSe substrate. The dimensions of the single rings were as follows: $d = 335 \pm 26$ nm, thickness $= 34 \pm 5$ nm, and $h = 114 \pm 19$ nm ($N = 7$). The dimensions of the double rings were as follows: $d_{\text{inner ring}} = 330 \pm 19$ nm, $\text{thickness}_{\text{inner ring}} = 40 \pm 5$ nm, $d_{\text{outer ring}} = 725 \pm 48$ nm, $\text{thickness}_{\text{outer ring}} = 38 \pm 8$ nm, and $h = 137 \pm 10$ nm ($N = 7$). The diameter of the outer ring in the direction of cutting was 10% smaller than it was along the perpendicular, uncompressed axis because the PPy spacer layer was more compressible than was the epoxy matrix. The compression of the inner ring was insignificant. The source of irradiation was a focused globar, which was polarized perpendicular to the compressed axis (direction of cutting). We placed the sample at the beam waist to approximate excitation by a plane-wave. The transmission spectrum of the single rings displayed one dip in transmission, while the spectrum of the double rings exhibited two (Figure 5a). These features in the spectra corresponded to the dipole resonances of the rings.[44] As expected, the smaller ring produced a higher energy resonance ($\lambda \sim 2.5$ μm) than did the larger ring ($\lambda \sim 5$ μm). The positions of the resonances in the results of the FDTD simulations approximately matched those of the measured spectra (Figure 5b). Figure 5c shows the simulated intensities of the electric field in the near-field for each of the dipolar resonances of the rings.

We attribute the red shift of the resonances in the experimental spectra relative to those of the simulated spectra to the mechanical deformation of the rings into ellipses during sectioning. Because the polarization of the excitation light was perpendicular to the compression direction, the incident light encountered a slightly larger effective ring diameter. This effect had the consequence of red-shifting the resonances compared to those found in the simulated spectra. Furthermore, the higher-wavelength resonance is more red-shifted than the lower-wavelength resonance because the PPy

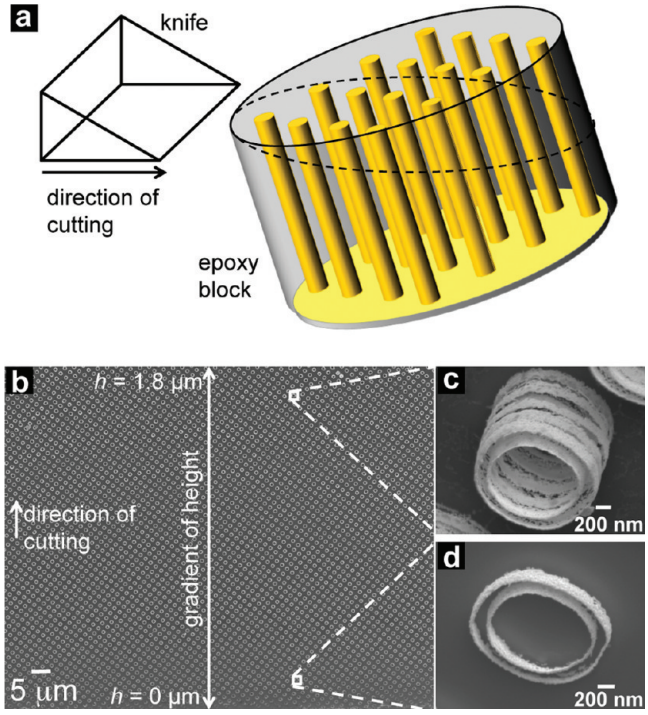

Figure 6. Fabrication of structures with a gradient of heights by obtaining wedge-shaped slabs of nanopost arrays. (a) Schematic illustration of the process. (b–d) Array of stacked concentric rings with inner diameters of ~1 μm. We achieved partial separation of the rings by evaporating against microposts with corrugated side walls (see Figure 2b) at normal incidence; this procedure deposited metal only on the wide segments of the microposts.

spacer layer between the two rings was more compressible than the epoxy encircled by the inner ring. Nevertheless, the closeness of the experimental and theoretical results demonstrates that nanoskiving produces structures of sufficient quality for optical applications.

While the experimental and simulated results match well for the dips in transmission due to the smaller ring, the dip in transmission due to the larger ring is broader and less intense in the experimental data than in the FDTD simulations. We attribute this effect to the reduced quality (*e.g.*, roughness and holes; see Figure 3d) of the gold film deposited on the PPy sacrificial layer, which forms the larger ring. The decrease in the quality of the film reduces the quality factor of the resonant mode and also reduces the homogeneity of the rings with respect to the other rings in the array. Both of these effects can decrease the amplitude and increase the width of a resonance. In general, the roughness should not change the overall shape of the resonances, provided the roughness is small compared to the wavelength. The effect of point defects depends on the nature of the defect. For example, rings of slightly different sizes will resonate at different frequencies, and the global resonances observed will again be wider and shallower than in the ideal case (inhomogeneous broadening). Possible methods to improve the quality of the film of the larger ring would be to use a sacrificial material whose morphology is easier to control than is that of PPy (*e.g.*, silicon dioxide, etched by HF or CF_3H, or amorphous silicon, etched by XeF_2). The simulated spectra represent the responses of 5 × 5 arrays of structures (see the Supporting Information for details of the optical characterization and FDTD simulations).

Fabrication of Arrays with Gradients of Height and 3D Nanostructures. Figure 6a is a schematic illustration of the procedure used to generate arrays of nanostructures with a continuous gradient of height. Tilting the block face forward by ~2° with respect to the diamond knife produced a wedge-shaped slab with a continuous increase in height from 0 to up to 2 μm. Figure 6b is an array of concentric cylinders formed from microposts. Figure 6c,d shows images taken at tilt of 45° from the thick and thin regions, respectively. The effect of the corrugated side walls of the posts (see Figure 2b, inset) produced the structure shown in Figure 6c—the gold film collected on the thick parts of the epoxy posts. Such an approach, similar to "side wall corrugation lithography",[45] could be used to generate more sophisticated 3D structures.[17]

Limiting Factors. There are several factors that limit the types of structures that can be made by molding, thin-film deposition, and sectioning. The resolution of EBL combined with the Bosch process limits the geometries and sizes of structures that can be made. The use of the perimeters of molded features limits the structures to line segments that cannot cross. There is also a trade-off between the pitch and the heights of the molded features: features that are too tall must be separated in order to permit collimated beams of metal atoms to reach the bottoms of the posts. The mechanical properties of thin films, in principle, limit the materials that can be used; we have observed, for example, that hard metals (*e.g.*, platinum) fracture more extensively than soft metals (*e.g.*, gold). The rough edges and holes in the side walls of some structures are traits of the underlying roughness of the epoxy features, as well as the conditions used for physical vapor deposition. We have found that ultrasonic, oscillating knives produce smoother features than stationary knives, but these knives exacerbate the effects of chips in the knives, by spreading their damage over a path whose width equals the amplitude of oscillation (~400 nm).[46] Preliminary observations suggest that the speed of cutting, between the programmable range of 0.1–10 mm/s, has no effect on the frequency of defects. We believe that further optimization of the process could yield struc-

tures with qualities close to those produced by conventional lithography.

CONCLUSIONS

The combination of processes described in this paper—replica molding of high-aspect-ratio nanoposts, deposition of thin films, and nanoskiving—provides an effective new means of replicating arrays of nanostructures over areas 1 mm^2. (The maximum area is limited, at present, to the size of the available diamond knives.) The geometries of individual nanostructures are not limited to circles and semicircles, such as those demonstrated in this paper. Rather, the perimeter of essentially any structure defined by lithography, and etching, can form a pattern by nanoskiving. Angle-dependent deposition and the use of sacrificial thin films as spacers can generate complex geometries comprising two or more materials in the same array. Any material that can be deposited on an epoxy replica by evaporation, sputtering, electrochemical growth, or drop-casting can define the composition of the final array of nanostructures. We have demonstrated structures composed of metals, semiconductors, dielectrics, and conducting polymers, singly or in combination with each other, in a variety of geometries, with low or high aspect ratios, and cut as many as 60 contiguous arrays from a single embedded structure.

We believe the combination of molding and nanoskiving has the potential to produce structures for metamaterials, sensing based on SERS or LSPR, and for basic study of optical properties of structures that cannot be made using existing methods (*e.g.*, very high-aspect-ratio structures, or those comprising two or more materials in the same plane). The closeness of the experimental data to the FDTD simulations for the arrays of single and double rings suggests that at least the basic optical properties of these arrays are calculable and predictable. The extent to which desirable properties can be programmed into the structures depends on the error introduced by rough edges and quality of the films, damage to the structures due to mechanical cleavage, and the thickness-dependent compression in the direction of cutting. We believe that the production of masters whose relief features have arbitrary geometries and smooth side walls, the deposition of smooth thin films, and proficient use of the ultramicrotome will enable the production of a large number of structures for basic research and eventual applications.

The most important impediment to transforming nanoskiving from a technique for research to one of manufacturing is replacing the manual steps—rough cutting the arrays to a size small enough (~1 mm × 1 mm) for the knife of the ultramicrotome, aligning the embedded structures with the knife edge, and collecting the sections from the water-filled trough—with automated procedures. The manual steps contribute to slab-to-slab variability. Differences in the slabs cut at different depths within the arrays of nanoposts arise from the imperfect, manual alignment of the embedded array to the edge of the knife, and plastic deformation (bowing) of the array while rough cutting and embedding. A recent technological development—reel-to-reel lathing ultramicrotomy—stands out as potentially useful for high-throughput and large-area nanoskiving.[47] The use of custom knives longer than 4 mm could also enable fabrication over larger areas than is possible with knives designed for small-area sections for transmission electron microscopy.

One of the original motivations for developing nanoskiving was to provide a simple method of making nanostructures similar to those that could, in principle, be made by scanning-beam lithographies, such as EBL and FIB.[32] Nanoskiving would thus be a simple, alternative method of nanofabrication accessible to general users in fields outside of electrical engineering and solid-state physics, such as chemistry and biology. This paper, however, demonstrates that the combination of characteristics of arrays of structures formed by nanoskiving—multimaterial, high-aspect-ratio, three-dimensional, flexible, manipulable, and replicable—are not found in structures formed by other techniques. We believe that research on plasmonic materials is the area to which the structures produced by nanoskiving can be most quickly applied, though there could be other applications in, for example, surfaces with engineered interfacial properties[48] and devices for energy conversion and storage.[9,49] Nanoskiving might, ultimately, suggest new ways of nanomanufacturing by cutting.

Acknowledgment. This research was supported by the National Science Foundation under award PHY-0646094. F.C. acknowledges a DOD/DARPA Contract Award No. HR 0011-06-1-0044. The authors used the shared facilities supported by the NSF under MRSEC (DMR-0213805 and DMR-0820484). This work was performed in part using the facilities of the Center for Nanoscale Systems (CNS), a member of the National Nanotechnology Infrastructure Network (NNIN), which is supported by the National Science Foundation under NSF Award No. ECS-0335765. CNS is part of the Faculty of Arts and Sciences at Harvard University. D.J.L. acknowledges a Graduate Fellowship from the American Chemical Society, Division of Organic Chemistry, sponsored by Novartis. The authors acknowledge Romain Blanchard and Benjamin Wiley for helpful discussions, Ludovico Cademartiri for synthesizing the PbS nanocrystals, and Christian Pflugl for assistance with the optical setup and general advice.

Supporting Information Available: Details of the fabrication, optical characterization, and simulation. This material is available free of charge *via* the Internet at http://pubs.acs.org.

REFERENCES AND NOTES

1. Maier, S. A; Atwater, H. A. Plasmonics: Localization and Guiding of Electromagnetic Energy in Metal/Dielectric Structures. *J. Appl. Phys.* **2005**, *98*, 011101.
2. Love, J. C.; Paul, K. E.; Whitesides, G. M. Fabrication of Nanometer-Scale Features by Controlled Isotropic Wet Chemical Etching. *Adv. Mater.* **2001**, *13*, 604–607.
3. Wu, D. M.; Fang, N.; Sun, C.; Zhang, X.; Padilla, W. J.; Basov,

D. N.; Smith, D. R.; Schultz, S. Terahertz Plasmonic High Pass Filter. *Appl. Phys. Lett.* **2003**, *83*, 201–203.
4. Sharma, A. K.; Jha, R.; Gupta, B. D. Fiber-Optic Sensors Based on Surface Plasmon Resonance: A Comprehensive Review. *IEEE Sens. J.* **2007**, *7*, 1118–1129.
5. Kneipp, K.; Kneipp, H.; Itzkan, I.; Dasari, R. R.; Feld, M. S. Surface-Enhanced Raman Scattering and Biophysics. *J. Phys.: Condens. Matter* **2002**, *14*, R597–R624.
6. Smythe, E. J.; Dickey, M. D.; Bao, J. M.; Whitesides, G. M.; Capasso, F. Optical Antenna Arrays on a Fiber Facet for *In Situ* Surface-Enhanced Raman Scattering Detection. *Nano Lett.* **2009**, *9*, 1132–1138.
7. Liu, X. F.; Sun, C. H.; Linn, N. C.; Jiang, B.; Jiang, P. Wafer-Scale Surface-Enhanced Raman Scattering Substrates with Highly Reproducible Enhancement. *J. Phys. Chem. C* **2009**, *113*, 14804–14811.
8. Fort, E.; Gresillon, S. Surface Enhanced Fluorescence. *J. Phys. D: Appl. Phys.* **2008**, *41*, 013001.
9. Atwater, H. A.; Polman, A. Plasmonics for Improved Photovoltaic Devices. *Nat. Mater.* **2009**, *9*, 205–213.
10. Peumans, P.; Bulovic, V.; Forrest, S. R. Efficient Photon Harvesting at High Optical Intensities in Ultrathin Organic Double-Heterostructure Photovoltaic Diodes. *Appl. Phys. Lett.* **2000**, *76*, 2650–2652.
11. Klar, T. A.; Kildishev, A. V.; Drachev, V. P.; Shalaev, V. M. Negative-Index Metamaterials: Going Optical. *IEEE J. Sel. Top. Quantum Electron.* **2006**, *12*, 1106–1115.
12. Cubukcu, E.; Yu, N. F.; Smythe, E. J.; Diehl, L; Crozier, K. B.; Capasso, F. Plasmonic Laser Antennas and Related Devices. *IEEE J. Sel. Top. Quantum Electron.* **2008**, *14*, 1448–1461.
13. Pendry, J. B.; Holden, A. J.; Robbins, D. J.; Stewart, W. J. Magnetism From Conductors and Enhanced Nonlinear Phenomena. *IEEE Trans. Microwave Theory Tech.* **1999**, *47*, 2075–2084.
14. Valentine, J.; Zhang, S.; Zentgraf, T.; Ulin-Avila, E.; Genov, D. A.; Bartal, G.; Zhang, X. Three-Dimensional Optical Metamaterial with a Negative Refractive Index. *Nature* **2008**, *455*, 376–380.
15. Pendry, J. B. Negative Refraction Makes a Perfect Lens. *Phys. Rev. Lett.* **2000**, *85*, 3966–3969.
16. Pendry, J. B.; Schurig, D.; Smith, D. R. Controlling Electromagnetic Fields. *Science* **2006**, *312*, 1780–1782.
17. Liu, N.; Guo, H. C.; Fu, L. W.; Kaiser, S.; Schweizer, H.; Giessen, H. Three-Dimensional Photonic Metamaterials at Optical Frequencies. *Nat. Mater.* **2008**, *7*, 31–37.
18. Gansel, J. K.; Thiel, M.; Rill, M. S.; Decker, M.; Bade, K.; Saile, V.; von Freymann, G.; Linden, S.; Wegener, M. Gold Helix Photonic Metamaterial as Broadband Circular Polarizer. *Science* **2009**, *325*, 1513–1515.
19. Stewart, M. E.; Anderton, C. R.; Thompson, L. B.; Maria, J.; Gray, S. K.; Rogers, J. A.; Nuzzo, R. G. Nanostructured Plasmonic Sensors. *Chem. Rev.* **2008**, *108*, 494–521.
20. Xia, Y.; Xiong, Y. J.; Lim, B.; Skrabalak, S. E. Shape-Controlled Synthesis of Metal Nanocrystals: Simple Chemistry Meets Complex Physics. *Angew. Chem., Int. Ed.* **2009**, *48*, 60–103.
21. Ahmadi, A.; Ghadarghadr, S.; Mosallaei, H. An Optical Reflectarray Nanoantenna: The Concept and Design. *Opt. Express* **2010**, *18*, 123–133.
22. Haynes, C. L.; Van Duyne, R. P. Nanosphere Lithography: A Versatile Nanofabrication Tool for Studies of Size-Dependent Nanoparticle Optics. *J. Phys. Chem. B* **2001**, *105*, 5599–5611.
23. Gwinner, M. C.; Koroknay, E.; Fu, L. W.; Patoka, P.; Kandulski, W.; Giersig, M.; Giessen, H. Periodic Large-Area Metallic Split-Ring Resonator Metamaterial Fabrication Based on Shadow Nanosphere Lithography. *Small* **2009**, *5*, 400–406.
24. Paul, K. E.; Zhu, C.; Love, J. C.; Whitesides, G. M. Fabrication of Mid-Infrared Frequency-Selective Surfaces by Soft Lithography. *Appl. Opt.* **2001**, *40*, 4557–4561.
25. Stewart, M. E.; Mack, N. H.; Malyarchuck, V.; Soares, J. A. N. T.; Lee, T. W.; Gray, S. K.; Nuzzo, R. G.; Rogers, J. A. Quantitative Multispectral Biosensing and 1D Imaging Using Quasi-3D Plasmonic Crystals. *Proc. Natl. Acad. Sci. U.S.A.* **2006**, *103*, 17143–17148.
26. Henzie, J.; Barton, J. E.; Stender, C. L.; Odom, T. W. Large-Area Nanoscale Patterning: Chemistry Meets Fabrication. *Acc. Chem. Res.* **2006**, *39*, 249–257.
27. Lee, J.; Hasan, W.; Stender, C. L.; Odom, T. W. Pyramids: A Platform for Designing Multifunctional Plasmonic Particles. *Acc. Chem. Res.* **2008**, *41*, 1762–1771.
28. Tserkezis, C.; Papanikolaou, N.; Gantzounis, G.; Stefanou, N. Understanding Artificial Optical Magnetism of Periodic Metal-Dielectric-Metal Layered Structures. *Phys. Rev. B* **2008**, *78*, 165114.
29. Su, K. H.; Durant, S.; Steele, J. M.; Xiong, Y.; Sun, C.; Zhang, X. Raman Enhancement Factor of a Single Tunable Nanoplasmonic Resonator. *J. Phys. Chem. B* **2006**, *110*, 3964–3968.
30. Engheta, N. Circuits with Light at Nanoscales: Optical Nanocircuits Inspired by Metamaterials. *Science* **2007**, *317*, 1698–1702.
31. Hoffman, P.; Utke, I.; Perentes, A.; Bret, T.; Santschi, C.; Apostolopoulos, V. Comparison of Fabrication Methods of Sub-100 nm Nano-Optical Structures and Devices. *Proc. SPIE* **2007**, 5925.
32. Xu, Q. B.; Rioux, R. M.; Dickey, M. D.; Whitesides, G. M. Nanoskiving: A New Method To Produce Arrays of Nanostructures. *Acc. Chem. Res.* **2008**, *41*, 1566–1577.
33. Gates, B. D.; Xu, Q. B.; Stewart, M.; Ryan, D.; Willson, C. G.; Whitesides, G. M. New Approaches to Nanofabrication: Molding, Printing, and Other Techniques. *Chem. Rev.* **2005**, *105*, 1171–1196.
34. Xu, Q. B.; Bao, J. M.; Rioux, R. M.; Perez-Castillejos, R.; Capasso, F.; Whitesides, G. M. Fabrication of Large-Area Patterned Nanostructures for Optical Applications by Nanoskiving. *Nano Lett.* **2007**, *7*, 2800–2805.
35. Pokroy, B.; Epstein, A. K.; Persson-Gulda, M. C. M.; Aizenberg, J. Fabrication of Bioinspired Actuated Nanostructures with Arbitrary Geometry and Stiffness. *Adv. Mater.* **2009**, *21*, 463–469.
36. Xu, Q. B.; Mayers, B. T.; Lahav, M.; Vezenov, D. V.; Whitesides, G. M. Approaching Zero: Using Fractured Crystals in Metrology for Replica Molding. *J. Am. Chem. Soc.* **2005**, *127*, 854–855.
37. McAuley, S. A.; Ashraf, H.; Atabo, L.; Chambers, A.; Hall, S.; Hopkins, J.; Nicholls, G. Silicon Micromachining Using a High-Density Plasma Source. *J. Phys. D: Appl. Phys.* **2001**, *34*, 2769–2774.
38. Jesior, J. C. How to Avoid Compression—A Model Study of Latex Sphere Grid Sections. *J. Ultrastruct. Res.* **1985**, *90*, 135–144.
39. Jesior, J. C. How to Avoid Compression 2—The Influence of Sectioning Conditions. *J. Ultrastruct. Mol. Struct. Res.* **1986**, *95*, 210–217.
40. Yee, K. S. Numerical Solution of Initial Boundary Value Problems Involving Maxwell's Equations in Isotropic Media. *IEEE Trans. Antennas Propag.* **1966**, *AP14*, 302.
41. Taflove, A.; Hagness, S. C. *Computational Electrodynamics: The Finite-Difference Time-Domain Method*; Artech House Publishers: Boston, MA, 2005.
42. Xu, Q.; Rioux, R. M.; Whitesides, G. M. Fabrication of Complex Metallic Nanostructures by Nanoskiving. *ACS Nano* **2007**, *1*, 215–227.
43. Cademartiri, L.; von Freymann, G.; Arsenault, A. C.; Bertolotti, J.; Wiersma, D. S.; Kitaev, V.; Ozin, G. A. Nanocrystals as Precursors for Flexible Functional Films. *Small* **2005**, *1*, 1184–1187.
44. Aizpurua, J.; Hanarp, P.; Sutherland, D. S.; Kall, M.; Bryant, G. W.; de Abajo, F. J. G. Optical Properties of Gold Nanorings. *Phys. Rev. Lett.* **2003**, *90*, 057401.
45. Kostovski, G.; Mitchell, A.; Holland, A.; Austin, M. Sidewall Corrugation Lithography: Bulk Fabrication of Ordered Nanowires, Nanoribbons, and Nanorings. *Appl. Phys. Lett.* **2008**, *92*, 057401.

46. Studer, D.; Gnaegi, H. Minimal Compression of Ultrathin Sections with Use of an Oscillating Diamond Knife. *J. Microsc. Oxford* **2000**, *197*, 94–100.
47. Kasthuri, N.; Hayworth, K.; Tapia, J. C.; Schalek, R.; Nundy, S.; Lichtman, J. W. The Brain on Tape: Imaging an Ultra-Thin Section Library (UTSL). *Soc. Neurosci. Abstr.* **2009**.
48. Pokroy, B.; Kang, S. H.; Mahadevan, L.; Aizenberg, J. Self-Organization of a Mesoscale Bristle into Ordered, Hierarchical Helical Assemblies. *Science* **2009**, *323*, 237–240.
49. Lipomi, D. J.; Chiechi, R. C.; Reus, W. F.; Whitesides, G. M. Laterally Ordered Bulk Heterojunction of Conjugated Polymers: Nanoskiving a Jelly Roll. *Adv. Funct. Mater.* **2008**, *18*, 3469–3477.